GEOPHYSICS, VOL. 76, NO. 2 (MARCH-APRIL 2011); P. B33–B42, 12 FIGS.
10.1190/1.3537822

Case History

Recursive imaging with multiply scattered waves using partial image regularization: A North Sea case study

Alison E. Malcolm[1], Maarten V. De Hoop[2], and Bjørn Ursin[3]

ABSTRACT

As more resources are directed toward reverse time migration, an accurate velocity model, including strong reflectors, is necessary to form a clear image of the subsurface. This is of particular importance in the vicinity of salt, where singly scattered waves are often not ideal for imaging the salt flanks. This has led to interest in processing doubly scattered waves (also called duplex or prismatic waves) for imaging salt flanks and thus improving the location of salt boundaries in a velocity model. We used doubly scattered waves in a two-pass, one-way method to image salt flanks in a North Sea data set. By working in the one-way framework we were able to separately construct images with singly, doubly, and triply scattered waves. We used a multistep imaging process that includes multiply scattered waves by using an imaged reflector to fix one (or more) of the scattering points, allowing for multiply scattered energy from several reflectors, potentially with poor continuity, to be included without picking each reflector individually. With this method we were able to image the flank of a North Sea salt body.

INTRODUCTION

In two related papers, Farmer et al. (2006) and Jones et al. (2007) show how so-called prismatic reflections (doubly scattered waves) can be included in a reverse-time-migration procedure by including a reflector in the velocity model to improve the location of salt flanks in a North Sea data set. We use the same data set to demonstrate a recursive, data-driven, one-way approach introduced in Malcolm et al. (2009). There are several advantages to using such an approach for this imaging problem. The first is that in the recursive approach a standard image (i.e., an image made with a standard migration algorithm assuming that all of the recorded signal comes from singly scattered waves) is used as an estimate of the location and amplitude of the multiple-generating interface, removing the need to pick a reflector and include it in the background velocity model; for the data set used in this study, this moves the imaged salt flank. (We will use the word "multiple" here to refer to any wave that has scattered more than once; thus, doubly scattered, prismatic, or duplex waves are considered multiples.) In addition, by imaging in a one-way approach we have control of the various wave constituents and their direction of propagation. This allows separate images to be produced from singly, doubly, and triply scattered waves; the total image is obtained as the sum of these contributions. It is then possible to interpret these images separately and to highlight and remove any artifacts from each of them. The use of one-way methods, although limited somewhat in terms of high-angle accuracy, reduces the computational cost of the procedure.

Doubly scattered waves, referred to as either duplex waves or prismatic reflections in the literature, have been considered as a source of additional information for some time. Bell (1991) uses them to explicitly locate a vertical reflector by reducing the traveltime of a doubly scattered wave to that of a primary. The effect of doubly scattered waves on dip moveout algorithms is discussed by Hawkins (1994). Bernitsas et al. (1997) demonstrate artifacts expected in subsalt imaging from prismatic reflections. In a more modern imaging context, Marmalevskyi et al. (2005) uses a ray-theoretic approach and an explicitly

Manuscript received by the Editor 27 February 2010; revised manuscript received 8 August 2010; published online 7 March 2011.
[1]Massachusetts Institute of Technology, Department of Earth, Atmospheric and Planetary Sciences, Cambridge, Massachusetts, U.S.A. E-mail: amalcolm@mit.edu.
[2]Purdue University, Department of Mathematics and Department of Earth Sciences, West Lafayette, Indiana, U.S.A. E-mail: mdehoop@math.purdue.edu.
[3]Norwegian University of Science and Technology, Department of Petroleum Engineering and Applied Geophysics, Trondheim, Norway. E-mail: bjorn.ursin@ntnu.no.
© 2011 Society of Exploration Geophysicists. All rights reserved.

Downloaded 22 Jun 2011 to 72.93.188.223. Redistribution subject to SEG license or copyright; see Terms of Use at http://segdl.org/

picked near-horizontal reflector to image a near-vertical reflector with doubly scattered waves; this is adapted and applied to a field data set by Link et al. (2007). The work of Broto and Lailly (2001) and Cavalca and Lailly (2005, 2007) also uses ray theory and doubly scattered waves but in the context of developing an inversion algorithm that allows for regions in which particular events are not recorded or do not exist (they used doubly scattered waves as an example of when this might occur). Most recently, Marmalevskyi et al. (2008) and Kostyukevych et al. (2009) compute transmission coefficients for doubly scattered waves to allow their migration in a Kirchhoff method for a vertical seismic profiling (VSP) geometry in fractured media.

Our method for imaging with multiply scattered waves has similarities to the two-pass, one-way methods proposed first by Hale et al. (1991) for imaging turning waves, in which the wavefield is first propagated down into the subsurface and stored at depth and then propagated back to the surface in a second pass. More recent discussions of this method can be found in Xu and Jin (2006) and Zhang et al. (2006). Doubly scattered wave imaging differs from turning wave imaging by its inclusion of a reflection from the lower boundary. This was done using the multiple-forward, single-backscatter method in Jin et al. (2006) and Xu and Jin (2007). In contrast, rather than explicitly including this reflector in the velocity model, we use a standard image to approximate the strength and location of the multiple-generating reflector. Specifically, within a shot-record migration algorithm, we first propagate the wavefield down into the subsurface, then multiply by the reflectivity estimated from the standard image; the resulting composite wavefield is then propagated upward, and an image is formed from the interference of the source and data wavefields. The use of an image to approximate the location and strength of the multiple-generating reflector also sets our method apart from the reverse-time methods mentioned above (Farmer et al., 2006; Jones et al., 2007), in which the reflector is included in the velocity model. Our method assumes that multiples do not generate artifacts in this singly scattered image, which is equivalent to assuming that they either have been removed or arrive late enough to be unimportant.

There is no fundamental difference between imaging with doubly and triply scattered waves (e.g., internal or surface-related multiples). In practice to date, however, most imaging with multiply scattered waves has focused on surface-related multiples because these are the simplest to understand and the closest, in many ways, to singly scattered waves because the multiple-generating reflector is well known (e.g., sea surface). Beginning with the work of Reiter et al. (1991), who proposed a method for imaging with water-column multiples in a Kirchhoff scheme, and continuing through the recent work of Berkhout and Verschuur (2003, 2004, 2006), in which surface-related multiples are converted into primaries, surface-related multiples have been shown to provide added information for imaging. Brown and Guitton (2005) discuss a unified framework to image with primaries and surface-related multiples, focusing on removing crosstalk between the different images. There are also several discussions for particular acquisition configurations, such as VSP (Jiang, 2006) and ocean bottom cable (Muijs et al., 2007), as well as more in-depth inversion procedures, such as that suggested by Métivier et al. (2009). For the more-complicated situation of internal multiples, most studies exploiting these events rely on interferometry to record at depth and subsequently convert internal multiples into primaries (Schuster et al., 2004; Jiang et al., 2005, 2007; Vasconcelos et al., 2007). These methods are somewhat similar to the Berkhout and Verschuur (2006) methods in that they remove one leg of the propagation via crosscorrelation. Mittet (2002, 2006) discusses the inclusion of multiples in reverse time migration with a specific focus on data requirements for imaging multiples correctly without causing artifacts in the image. Youn and Zhou (2001) describe a method, based on finite differences, that allows for the simultaneous imaging of primaries and internal and surface-related multiples but that requires detailed velocity information and additional computational resources compared to those for other methods.

As is to be expected, when imaging with the relatively low-amplitude multiply scattered waves, data sampling becomes more important than for the singly scattered case. There are many different ways of interpolating data; a relatively recent review of different methods can be found in, e.g., Stolt (2002). Here we chose to use a combination of Fourier interpolation and curvelet-based thresholding. Curvelets, discussed in more detail in Candès et al. (2006), are a generalization of wavelets to multiple dimensions that are particularly well suited for wave problems; another example of a transform with similar properties is given in Duchkov et al. (2010). Using them for denoising is discussed in, e.g., Hennenfent and Herrmann (2006). Here we choose to use a hard threshold, (keeping only coefficients larger than this threshold).

This paper has three main sections; the first summarizes the method for imaging with multiples and the regularization method. The second uses synthetic data to illustrate sampling issues when imaging with multiply scattered waves, and the third discusses the application of the methods to a data set from the North Sea.

SUMMARY OF METHODS

The procedure for imaging with multiply scattered waves used here is discussed in detail in Malcolm et al. (2009); here we give a summary of the most important ideas, without discussing the underlying theory. The method builds on previous work in Malcolm and de Hoop (2005) that combines two series approaches: the generalized Bremmer series (de Hoop, 1996) and the Born series discussed by Weglein et al., (2003).

The basic structure of our technique for imaging with multiply scattered waves is straightforward. The procedure is broken into the following steps, illustrated in Figure 1.

1) Form a standard image, defined as a migrated image using any standard imaging technique that assumes singly scattered waves (Figure 1b).
2) Propagate the surface data down into the subsurface (with a one-way method), as in a standard shot-record migration. At each depth, multiply the wavefield by the image formed in step 1, and store the resulting composite wavefield at each depth (Figure 1c). This models the reflection of the wavefield from the multiple-generating interface, approximated by the image made in step 1.
3) Propagate the composite wavefield up to the surface (Figure 1c), forming an image at each depth by applying a crosscorrelation imaging condition to the two composite wavefields for internal multiples (illustrated in Figure 1e) and to one composite wavefield (traveling along the dashed path in Figure 1c) and the standard downward continued wavefield (traveling along the solid path in Figure 1c) for doubly scattered waves.

Downloaded 22 Jun 2011 to 72.93.188.223. Redistribution subject to SEG license or copyright; see Terms of Use at http://segdl.org/

As in reverse time migration, including multiples requires the specification of a layer boundary (or many boundaries) that generates the multiples (see the discussion in Jones et al. [2007]). In other words, referring to Figure 1, to make an image of R_2, an estimate of the reflectivity of R_1 is required. This information must be included directly in the velocity model for reverse time migration and for the methods of Jin et al. (2006) and Xu and Jin (2007). In our method this information is included separately and is obtained directly from a standard image because this is the best estimate we expect to have of the reflectivity itself. In this way, only the regions of the image (and, if the image is accurate, of the earth) that have significant reflectivity contribute to the generation of multiply scattered waves, and it is not necessary to specify explicitly any layers that may generate multiples. It is still possible to exclude multiples generated at specific layer boundaries by muting the input image to remove reflections from those layers; multiples generated at these muted layers will then not be included in the multiply scattered wave imaging. For all multiples, it is thus not necessary that there be a single coherent reflector that forms the R_1 imaging points in Figure 1; the image points could, instead, be generated by a group of less-coherent reflectors. There must still be something that physically reflects the energy toward the second scattering point on R_2 (in other words, multiples must be generated by the earth and recorded at the surface).

Similar to methods discussed by Brown and Guitton (2005), imaging with multiply scattered waves requires the separation of these multiples from primaries. Although a method such as that suggested by Brown and Guitton would likely result in a cleaner image with fewer artifacts, we have found that much simpler procedures are adequate, in particular for doubly scattered waves. For these waves, we observe that most of the artifacts come from the interference of doubly scattered waves with primaries that share part of the path of the doubly scattered waves, as illustrated (dashed rays) in Figure 1c. These waves can be removed in a straightforward manner by applying an *f-k* filter before applying the imaging condition to separate left- and right-going waves, thus allowing the imaging condition to be applied to wavefields traveling in opposite horizontal directions. In the example studied here, we find the best results using a filter that tapers to zero over several wavelengths, removing waves up to vertical propagation from the source- and receiver-side wavefields; we found that using a smooth filter is more important than the specific location of the cutoff wavenumber.

Regularization

When imaging near-vertical structures, it is quite important to form an image with sufficient lateral resolution to resolve the location and dip of these features. This may require resolution beyond that of a standard survey, and thus, we explore the possibility of interpolating the data to improve the lateral resolution. In addition, because the data are used twice in the imaging procedure (once to form the standard image and again to form the doubly scattered image), it is more important for this type of imaging than for standard imaging that the data contain mainly coherent events with a minimum of noise. This requirement indicates that some denoising, preserving, or even enhancing lateral continuity of events is desirable. To perform these tasks, we use a curvelet-based denoising and data regularization method. We would like to emphasize that this method does not necessarily result in a singly scattered image that is superior to a standard migrated image, in particular for interpretation. That is not our goal; our goal is to generate a standard image that when input into our double-scattered imaging procedure, improves the double scattered image.

The regularization method used here consists of two steps. First, the data are interpolated with a standard Fourier-based sinc interpolation, after which the curvelet-based denoising method is applied. The basic idea of this denoising method is to first compute the curvelet transform of the data (discussed in Candès et al. [2006]), which results in a decomposition of the data as a function of scale and orientation. Scale gives a measure of the size of a structure; structures that are coherent in space have large coefficients over all scales, whereas incoherent structures have small coefficients over a range of scales. Orientation indicates the direction of the wave packet. We then apply a thresholding procedure in which coefficients less than (in absolute value) a percentage of the maximum coefficient are set to zero. This is generally referred to as hard thresholding. One could also use the soft-thresholding procedure introduced in Daubechies and Teschke (2005) and extended by Hennenfent and Herrmann (2006). By removing scales with small coefficients, we remove incoherent energy because such energy will be spread over several scales and orientations with little energy in any one scale-orientation pair. Coherent energy, however, will be spread over only a few scale/orientation pairs, resulting in larger coefficients. This procedure is conceptually similar to low-pass filtering, although here the filter is applied in a domain

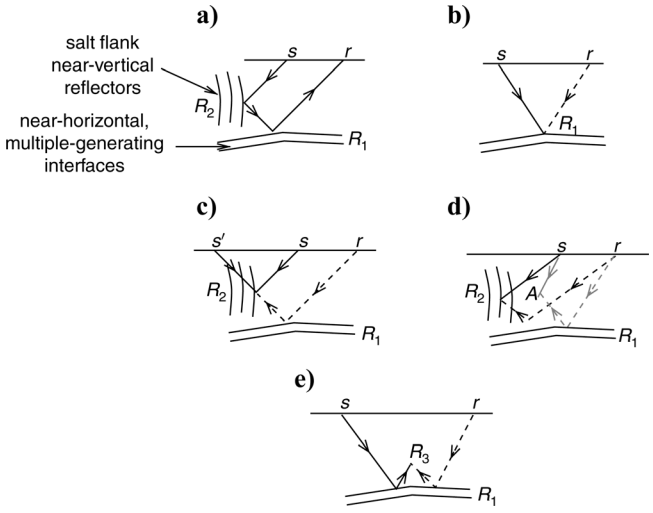

Figure 1. (a) Raypath for a doubly scattered wave, such as that used here to image the salt flank. (b) Computing the image of the near-horizontal reflector (R_1); the dashed line from r indicates reverse propagation. (c) Computing the image of the near-vertical reflectors (again, the dashed line denotes reverse propagation). The wavefield from s' will create an artifact in the doubly scattered image, so it is removed by *f-k* filtering. (d) Early arrivals in the data will create artifacts in the image at A, to the right of the proper image R_2. In this cartoon, waves actually propagate along the black path but are imaged as though they have traveled along the gray path. (e) For imaging with internal multiples, the source- and receiver-side wavefields are reflected from R_1, and an image is formed at the central scattering point by correlating the two fields (again, the dashed line denotes reverse propagation).

Downloaded 22 Jun 2011 to 72.93.188.223. Redistribution subject to SEG license or copyright; see Terms of Use at http://segdl.org/

specifically tailored to wave problems (meaning that seismic data are sparse in the curvelet domain). Because the data are sparse, it is reasonable to expect that relatively few coefficients should be required to represent the data in this domain, thus justifying setting the smaller coefficients to zero.

EFFECT OF SAMPLING

To illustrate the importance of sampling in the lateral direction, as discussed above, and to illustrate the algorithm's capabilities, we begin with a synthetic data set with several near-vertical layers (i.e., structures with very large dip) that is designed to mimic the structures seen in the field data set discussed in the following section. The velocity model for this data set is shown in Figure 2, along with a standard image made with a shot-record migration using a simple phase-shift propagator, performing the phase-shift separately for each velocity occurring in a horizontal slice. This is similar to the phase-shift-plus-interpolation propagator (Gazdag and Sguazzero, 1984) as well as to the propagators suggested in Ferguson and Margrave (2002). Although the cost is somewhat prohibitive when using many velocities, it is easy to implement, and we find this propagator to be sufficiently accurate for this data set. Either this propagator or a simple split-step propagator is used throughout this paper. Any other one-way propagator could be used in place of either of these methods, provided it estimates the wavefield sufficiently accurately; because it is not our goal to investigate propagators, we chose the simplest propagator to implement that gave reasonable results for the models used.

Resolving the different vertical layers in this model requires that the image be made on a relatively dense horizontal grid. Because the goal is to image nearly (and beyond) vertical layers, good lateral resolution is required to image and identify the different layers. This does not mean that more data are required than are used to make a standard image, only that the image may need to be formed on a denser grid than that on which the data are collected. The effect of grid size is illustrated in Figure 3. In Figure 3 two different receiver sampling intervals (receiver sampling is equivalent to image and computational grid sampling in the x-direction [lateral position]) are used to form the doubly scattered image, both of which are sufficient to see the flank of the salt, but the denser of which (in Figure 3b) exhibits shorter wavelengths. In general, such shorter wavelengths will result in a higher-resolution image. Here, because the model contains several layers too close together to be resolved at the frequencies used, we are still not able to clearly resolve these layers even with the shorter wavelengths, although some separation at the top of the leftmost layers is now visible. We also illustrate, by muting the recordings from every other receiver for all shots in the data set used to make the image in Figure 3b (thus reducing the receiver sampling but not the image or grid sampling), that more data are not required, as the images in Figure 3b and 3c are nearly equivalent (the maximum differences are approximately 0.5%). All three images have significant ringing. This ringing is caused by a combination of (1) the truncation of the *f-k* filter used to separate doubly scattered waves from primaries, (2) multiply reflected waves between the different vertical layers, and (3) the convolution of an extra wavelet from using an image as an estimate of reflectivity. We expect that the second cause is dominant because, as will be illustrated with a simpler synthetic in the discussion section, simpler models (in which cases 1 and 3 are unchanged) have significantly less ringing than the images made in this model or the field data set do.

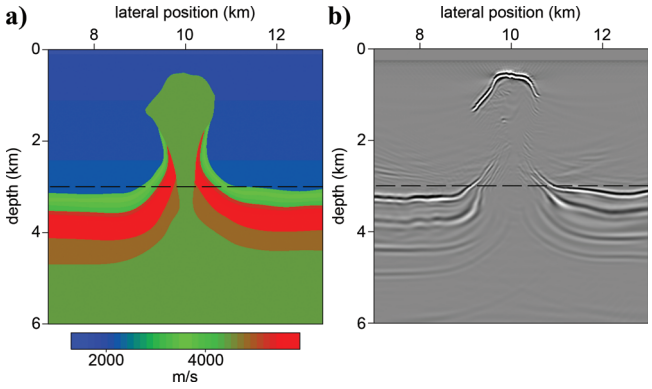

Figure 2. (a) Velocity model used to generate the synthetic data set. (b) Standard migration image made using data generated for the velocity model in (a), assuming single scattering, using a smoothed version (with 20-m radii in depth and lateral position) of the velocity model shown in (a).

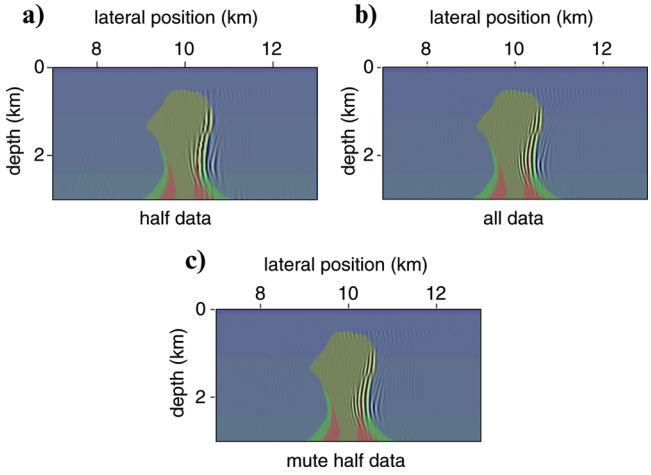

Figure 3. The effect of grid size on the final image. (a) A receiver spacing of 25 m (also the lateral position sampling of the image and computational grid) gives a good image of the vertical salt flank. (b) Using a receiver spacing of 12.5 m gives an image with shorter wavelength structures, although the location and shape of the reflector do not change much. (c) Using the same grid as in (b) for the propagation but with every second receiver muted (so an effective receiver spacing of 25 m with an actual receiver spacing [and image spacing and computational grid spacing in the lateral position] of 12.5 m) gives nearly the same image as in (b), indicating that the additional data are not required as long as the image is formed on a finer grid. All of these figures were made using the singly scattered migrated image shown in Figure 2b, muted outside the depth interval 2.5–3.4 km, as input and a 1D version (using the velocities at a lateral position of 7 km) of the velocity model shown in Figure 2a as the migration velocity model.

Downloaded 22 Jun 2011 to 72.93.188.223. Redistribution subject to SEG license or copyright; see Terms of Use at http://segdl.org/

APPLICATION TO NORTH SEA DATA SET

Now that we understand some of the advantages and limitations of the method with the synthetic data set used in the previous section, in this section we explore the possibility of using doubly scattered waves to improve the velocity model near a salt structure that is not well imaged. The data are from a North Sea field; this data set is discussed in more detail in Farmer et al. (2006) and Jones et al. (2007), where a similar set of procedures is applied in a reverse-time-migration framework. What our study adds is, first, the removal of the requirement that the salt itself be included in the velocity model and, second, the requirement that hard boundaries be included in the velocity model. The first requirement is removed by using only waves that travel outside the salt to image its boundaries. This is similar to the result in Jones et al. (2007) that used reverse time migration to image the salt flanks with duplex waves. The second requirement is removed by separating the smooth background velocity model, through which the waves are propagated, from the sharp interfaces from which the waves reflect. By using an image (for the reflectivity) and a velocity model (through which to propagate waves), we are able to reduce the requirements on the level of detail present in the migration velocity model. The velocity model, estimated through one-way tomography, as discussed in Jones et al. (2007), is shown in Figure 4a. The other figures shown of images made with this data set use either this model with the salt removed (sediment velocity model) or a 1D model consisting of the velocity as a function of depth at the first lateral position (approximately 127 km). The 1D model was used to test the influence of lateral variations in the model on the resulting images. Figure 4b shows an image made with all 315 recorded shots on a 2D line extracted from the 3D volume; the shot spacing is 50 m, and for each shot, 120 offsets are recorded with a minimum offset of 160 m and 25-m spacing. To avoid artifacts caused by waves traveling through the salt, we limit the offsets included in the imaging to 2 km; the image was made with a split-step propagator.

In the migrated image in Figure 4 the absence of reflections between lateral positions at approximately 129 and 133 km strongly suggests the presence of a salt dome in that region. To improve our ability to image this structure, we first form an image with doubly scattered waves using data recorded to the right of the salt, using 50 shots from 135 to 137.5 km. For doubly scattered waves, there are two reflections, one from the near-horizontal structures (R_1 in Figure 1) and another from the near-vertical structures (R_2 in Figure 1); by reciprocity, it makes no difference whether the waves travel from the surface to R_1 continuing to R_2 and then returning to the surface or travel first to R_2. To speed the computations, in forming a doubly scattered image for this side of the salt flank, we restricted the imaging procedure so that the reflection from the near-horizontal multiple-generating interface (R_1) is only on the receiver side (in other words, the waves travel from the source to R_2, continue to R_1, and are then recorded at the surface). Within the shot-record migration framework, this means that the reflection is included by back propagating the data wavefield, allowing it to reflect from the structure at R_1, and continuing to propagate upward. The source wavefield is propagated only forward, and an image is formed by interfering the down-going source wavefield with the upgoing receiver wavefield. This is consistent with the recording geometry, as the receivers are to the right of the source, precluding the recording of waves with the reciprocal travel path. The resulting image, made with the sediment velocity model, is shown in Figure 5 along with a similar image made in the 1D velocity model. Although these images give a clear indication of a salt flank, similar to that found in Jones et al. (2007), the ringing and the energy far from the expected salt flank detract from the image quality. The source of the ringing is likely the same as that in the synthetic example discussed above. We now discuss the attenuation of the energy farther from the salt flank; in attenuating it we also gain clues as to its origins.

The next step is to improve the lateral resolution of the image. On the basis of the discussion in the previous section, the image of the vertical structure can be improved by decreasing the grid size. Although, from that discussion, we expect that migrating on a finer grid without increasing the density of data sampling will improve the image, we decided to first regularize the data because of the large amount of energy far from the salt flank and high general noise level in the image. The regularization procedure used is that discussed in the methods section; here we used it to denoise and increase by a factor of five the receiver sampling (the regularized offset sampling is 5 m). An example of the resulting regularized data is shown in

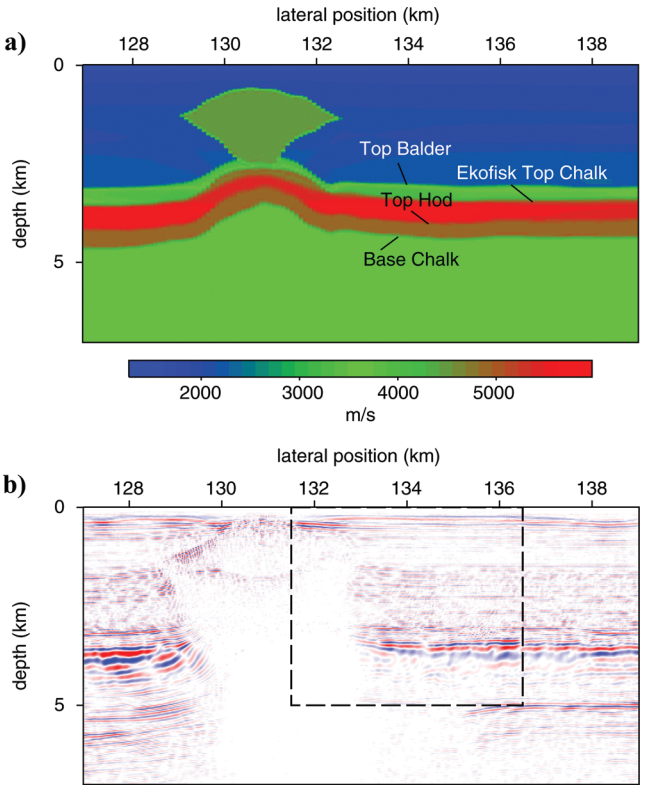

Figure 4. (a) Original velocity model for the real data set. Three different models are used in this case study: the full model, depicted here, the sediment model, which does not include the salt itself, and the 1D model, which is the velocity as a function of depth at the first lateral position (approximately 127 km). (b) Image made with the original data set, including offsets up to 2 km and using the sediment model.

Downloaded 22 Jun 2011 to 72.93.188.223. Redistribution subject to SEG license or copyright; see Terms of Use at http://segdl.org/

Figure 6, in which we see that the lateral continuity of the reflections is improved. The image formed from the regularized data, shown in Figure 7, shows an improvement over that shown in Figure 4b as an image to generate the first reflection R_1. Specifically, we note two differences that are key to our imaging goals. First, the reflector marked with an arrow has stronger amplitude relative to the reflectors above and below it; this reflector is likely one of the multiple-generating reflectors, and so improving its image is key to imaging with doubly scattered waves. Second, the reflectivity above this layer is significantly reduced. We expect that some of the artifacts seen in Figure 5 come from primaries and doubly scattered waves in these layers, as sketched in Figure 1d; their reduced amplitude in the regularized image indicates that we have also reduced their amplitude in the data, and thus, this image indicates that we can expect to be able to form a better doubly scattered image with the regularized data. We therefore classify this regularized image as better for our purposes, although it may not be better for all imaging applications. To image the flank of the salt or near-vertical chalk layer, believed to be against the salt flank, as in the synthetic model shown in Figure 2, we then repeat the double-scatter imaging with three different choices of velocity and single-scatter image pairs, the results of which are shown in Figure 8. Note that a significant fraction of the energy far from the salt flank has been removed. It is apparent that although the procedure depends on the input image and the initial velocity model, small changes in these inputs do not result in large changes in the final image.

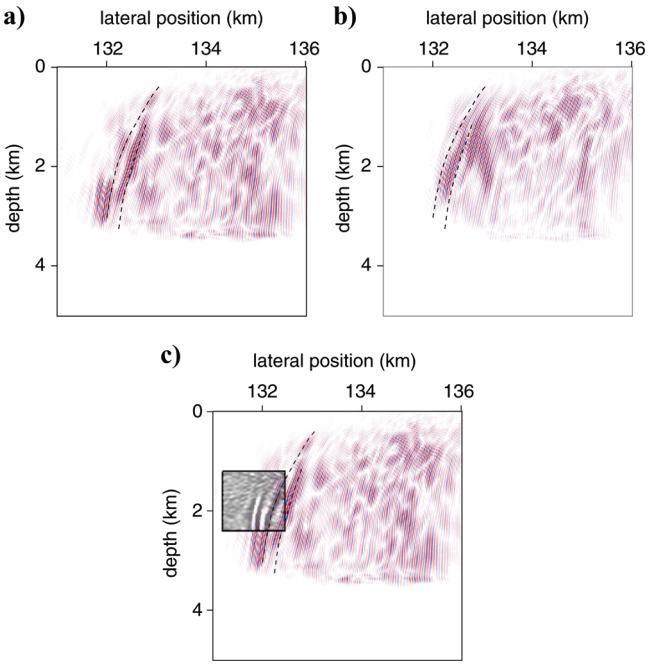

Figure 5. Doubly scattered images made with the original data, showing only the region of the model in the dashed box in Figure 4b and (a) the sediment velocity model and (b) the 1D velocity model. (c) The same as (a) but with the image in the box obtained in Jones et al. (2007). Dashed lines mark reflectors picked in Figure 10.

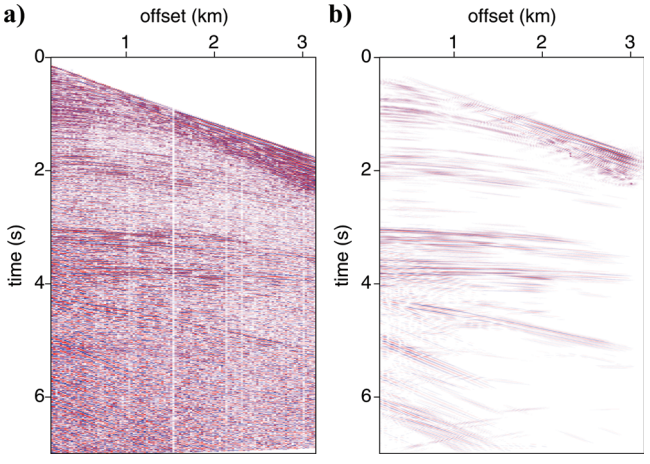

Figure 6. (a) Original shot record with shot at 135 km. (b) Shot record regularized and denoised.

The data regularization is able to decrease the amount of energy imaged far from the salt flanks, but the final image still exhibits what appear to be artifacts. Specifically, some energy remains relatively far from the expected salt-flank location. These artifacts could come from primaries or doubly scattered waves reflected from the layer boundaries with poor lateral continuity between the chalk layer and the water bottom, as illustrated in Figure 1d. If this is the case, then these events would arrive before reflections between the top of the chalk and the salt flank, so removing events that arrive before this time would be expected to reduce or even remove these artifacts. Additional evidence for this explanation of these artifacts is that they are not present in the synthetic data set, which models the deeper layers and multilayer salt flank structures but not the reflectivity between the upper layer and the water bottom. To remove this ringing, we use a surgical muting procedure to isolate, in the data, the doubly scattered energy between the top of the chalk layer and the salt flank. In the current framework, such a procedure is straightforward; first, we mute the double-scatter image to remove what we expect to be artifacts and to isolate what we think is the position of the vertical reflector (salt flank). Second, we isolate the top of the chalk in the regularized image in Figure 7, downsampled back to the original data sampling. We have now created an image of only the two reflectors involved

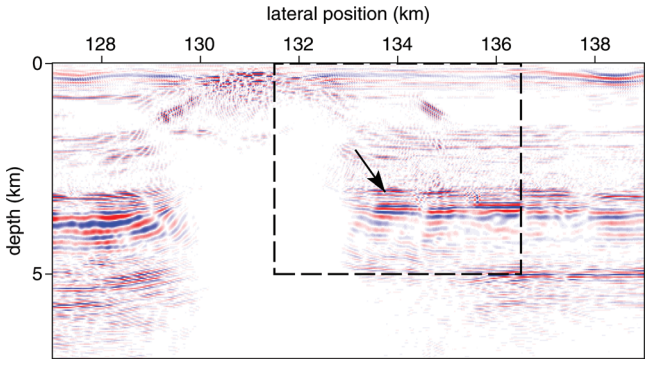

Figure 7. Image made with the regularized and denoised data and the sediment velocity model. The arrow indicates a reflector that is improved in the regularized image in that its amplitude is larger compared to surrounding layers.

Downloaded 22 Jun 2011 to 72.93.188.223. Redistribution subject to SEG license or copyright; see Terms of Use at http://segdl.org/

in the wave path of the doubly scattered energy we are trying to isolate. We then model the data using the sources that were used to form the image (in other words, using the same acquisition geometry as the original data) and changing the direction of the propagators. This results in a model of the doubly scattered waves in the data. We then perform a surgical mute on data, beginning within a few wavelengths of the modeled doubly scattered waves and keeping all data arriving after this time; by including data a few wavelengths prior to the modeled arrival times, this windowing allows for errors in the modeling from mispositioned reflectors and errors in the smooth velocity model but still isolates these events from others in the data. This muting process is illustrated in Figure 9. The resulting muted data set was then used to construct the doubly scattered image shown in Figure 10. Because this procedure has almost completely removed the energy to the right of the expected salt flank, we conclude that these artifacts must have come from events arriving before the doubly scattered waves that reflect from the salt flank. The most likely candidates for such energy seem to be events (either primaries or multiply scattered waves) generated by the somewhat discontinuous reflectors between the top of the chalk and the water bottom.

We then choose what we judge to be the best image of the salt flanks made with doubly scattered waves to add to the original standard migration images to form a final image of the entire region. These final images are shown in Figure 11. We stress that the entire imaging procedure was carried out without including the salt structure itself in the velocity model.

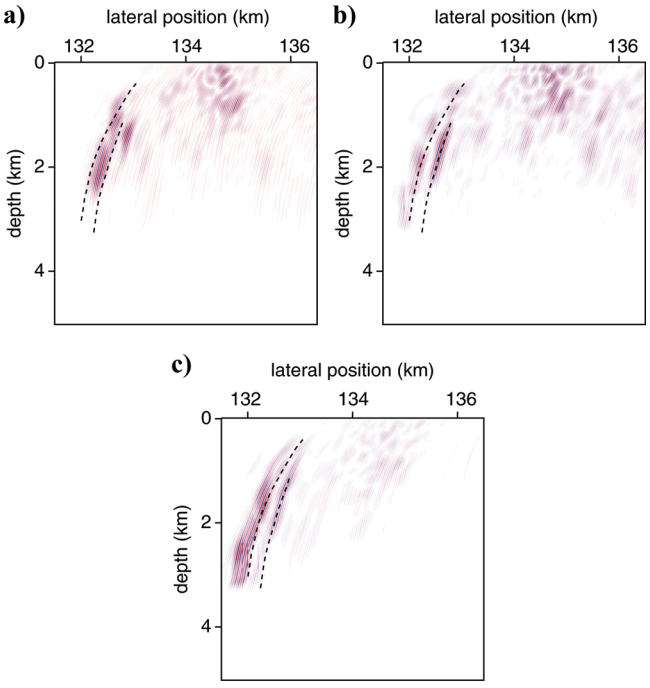

Figure 8. Images made with doubly scattered waves and the regularized data set, showing only the region in the dashed box in Figure 7. (a) Using the 1D velocity model using a muted version of the image in Figure 7a for the estimated reflectivity. (b) Using the sediment velocity model and a muted version of the image in Figure 7a for the estimated reflectivity. (c) Using the sediment velocity and a flat spike reflector at a depth of 3390 m for the reflectivity; this estimate of the reflectivity does not include a wavelet. The dashed lines mark the locations of the salt flanks as picked in Figure 10.

DISCUSSION

Throughout this paper, we have chosen to image only one side of the salt flank because the data set we obtained had data coverage for only one side of the reflector. Given equivalent source/receiver coverage, one could, of course, image either side using reciprocity. Motivated by a typical marine acquisition geometry, we study whether or not equivalent illumination of both

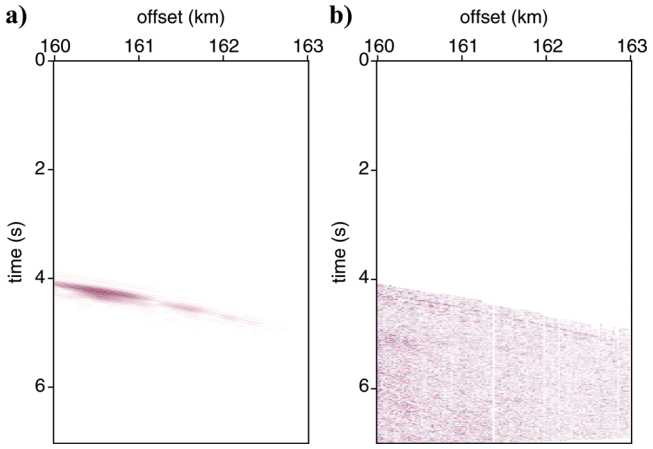

Figure 9. (a) Modeled doubly scattered data using the top-chalk reflector and the imaged salt flank as the two reflectors. (b) Original data muted with a mute designed to keep only the doubly scattered data and later arrivals, based on the modeled data in (a).

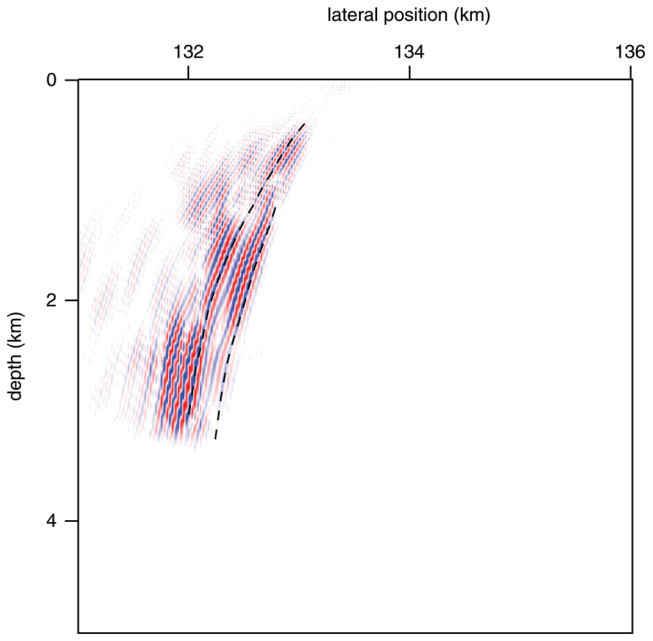

Figure 10. Doubly scattered image made with the surgically muted data, a muted version of the image in Figure 7a, and the sediment velocity model. Only the region of the image in the dashed box in Figure 4b is shown here. This figure should be compared with Figure 5.

Downloaded 22 Jun 2011 to 72.93.188.223. Redistribution subject to SEG license or copyright; see Terms of Use at http://segdl.org/

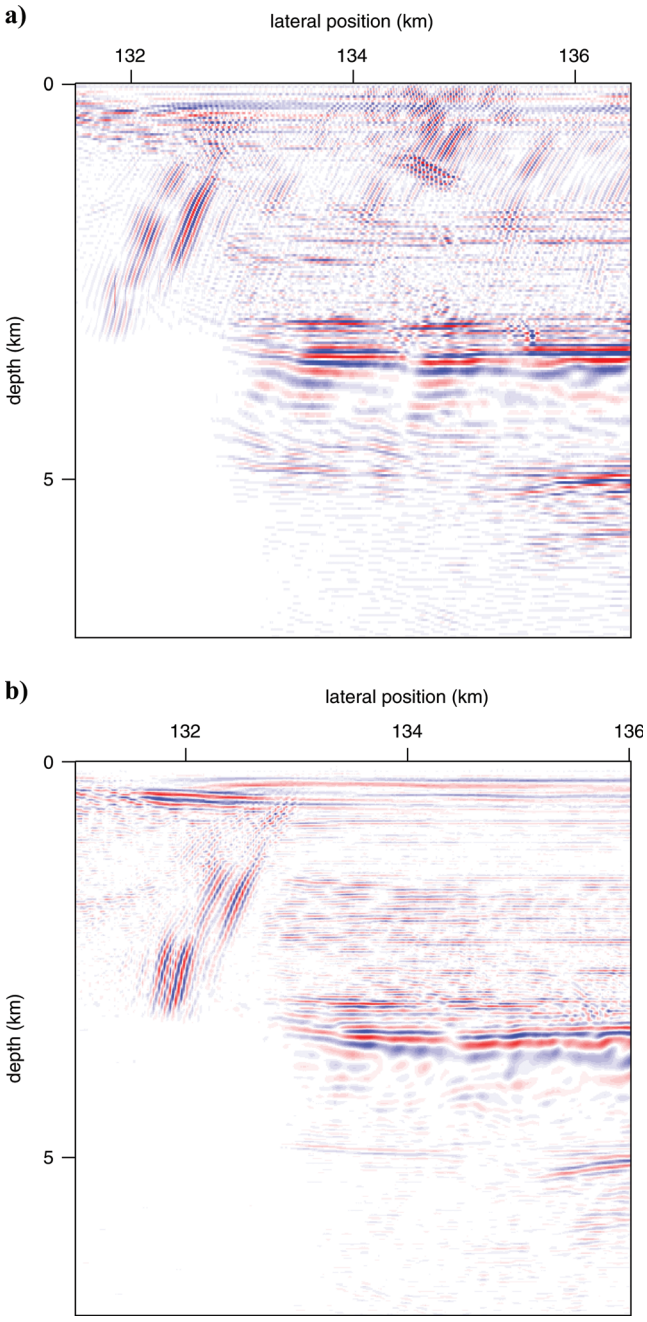

Figure 11. Total images, including singly and doubly scattered data, showing only the region of the image in the box in Figure 4b. (a) The regularized data set, using the image in Figure 7 muted outside 3.225- to 3.6-km depth as the estimated reflectivity. The remaining ringing at the salt flank (here and in [b]) may come from multiply scattered energy in vertical layers adjacent to the salt flank caused by the entrainment of sediment in the rising salt, similar to that depicted in the synthetic velocity model in Figure 2; the artifacts near the surface at around 134 km are likely from energy arriving before the main doubly scattered arrivals because they do not appear in (b), where this energy has been removed. (b) The unregularized data set, using the surgically muted data set to make the doubly scattered image and the image in Figure 4b muted outside of depths 3.225–3.6 km as the estimated reflectivity. Note that both images were made entirely with the sediment velocity model.

flanks of the salt is possible. To this end, we use a simple example in which a single near-vertical reflector is imaged. In this example, sources and receivers are simulated every 10 m, with 250 sources from 2.5 to 5 km and 250 receivers with offsets from 0 to 2.5 km. Figure 12 shows that there is little difference in the recovered image whether it is the sources or receivers that are decimated by a factor of 10, to a sampling of 100 m. This highlights the main difference between towing the streamer toward versus away from the flank to be imaged: the difference in sampling of the wave that reflects from the lower layer. This means that imaging with doubly scattered waves is possible whichever direction the streamer is towed. It is noteworthy, however, that data are required sufficiently far from the flank to allow the recording of doubly scattered waves. Large offsets are less important; the field data set discussed in this paper had offsets up to little more than 3 km, and only those up to 2 km were used to form the images. Doubly scattered waves, however, are not likely to be recorded near the salt flank for isolated salt domes such as the one used in this study. As mentioned above, the images shown in Figure 12 do not have the ringing seen in the previous synthetic and field data sets; this indicates that this ringing does not come from either convolution with an extra copy of the wavelet (because this data set uses the same wavelet as the previous synthetic example) or sharp cutoffs in the *f-k* filter used to separate multiples from primaries (because, again, the filter is the same for all examples in this study).

Although reverse time migration and full-waveform inversion are likely to make imaging with one-way methods obsolete in the near future, one-way methods still have a place in the estimation of the velocity near complicated structures. Even with the added complication of regularization and use of two-pass, one-way methods, it is still faster to make an image in this way than to use reverse-time methods. An added advantage of the ability to separate images made with singly, doubly, and triply scattered waves is that these separate images can be used to identify artifacts from crosstalk (as discussed in detail by Brown and Guitton [2005]), allowing an interpreter to assess the likely artifacts in each image separately. By using an image, rather than including the interface directly in the velocity model, one can still use discontinuous or poorly imaged structures to estimate and thus exploit multiply scattered waves. Methods such

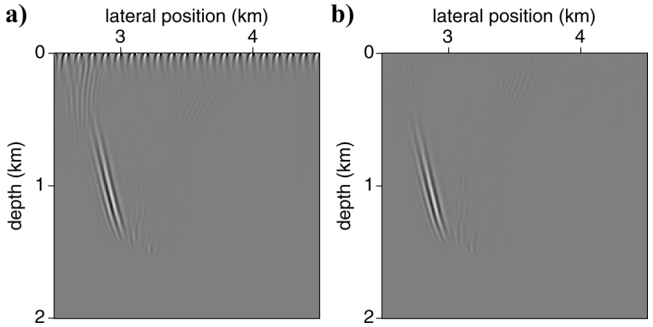

Figure 12. (a) Image of a steep simple curved reflector, made with only 10% of the original shot locations. (b) Same as (a), except that this time only 10% of the receivers were used, with the others muted (so the wave propagation is computed on the same grid for both plots).

Downloaded 22 Jun 2011 to 72.93.188.223. Redistribution subject to SEG license or copyright; see Terms of Use at http://segdl.org/

as the two-pass, one-way method of Hale et al. (1991) allow the imaging of steep reflectors with turning waves, when such waves are present in the data. The method discussed here, when used to image with doubly scattered waves, is complementary in that it allows for imaging of steeply dipping reflectors using a multiple-generating interface, rather than requiring a vertical velocity gradient. We could also use this methodology in an iterative manner to either update the salt location or improve the velocity model near to or below the salt; this is a subject of ongoing work.

CONCLUSIONS

We have shown that two-pass, one-way methods are able to image near-vertical structures such as salt flanks on field data, allowing improved understanding of the shape of these salt structures. Imaging with doubly scattered waves does not require particularly large offsets, but it does require data recorded at some distance from the structure of interest. Sampling is particularly important when imaging vertical structures with low-amplitude doubly scattered waves. We have shown that a curvelet-based regularization and denoising procedure applied to the data creates an image that is more amenable to use for the estimated reflectivity and that this data set also produces a doubly scattered image with fewer artifacts than that made with the original data. In this particular case, we found that designing a surgical muting procedure to isolate the doubly scattered phases of interest was helpful in removing additional imaging artifacts.

ACKNOWLEDGMENTS

We are grateful to GX Technologies for the data and permission to publish these results. In particular, Ivan Vasconcelos facilitated the data transfer and made several helpful suggestions, and Ian Jones helped to identify and extract a relevant 2D data subset and provided many of his own figures for comparison. In addition, Rune Mittet was particularly helpful in locating some difficult-to-find references. We thank Herwig Wendt and Shen Wang for help with the curvelet-based denoising procedure. We are grateful to Ken Larner for his careful review of this manuscript; his many insightful suggestions have greatly improved the presentation. B.U. would like to acknowledge financial support from Statoil through VISTA and the Norwegian Research Council through the ROSE project. M.V.d.H. was supported in part by the members of the Geo-Mathematical Imaging Group. A.M. acknowledges funding from Total and the sponsors of the Earth Resources Laboratory.

REFERENCES

Bell, D. W., 1991, Seismic imaging of steeply dipping geologic interfaces: U. S. Patent 4,987,561.

Berkhout, A. J., and D. J. Verschuur, 2003, Transformation of multiples into primary reflections: 73rd Annual Meeting, SEG, Expanded Abstracts, 1925–1928.

——, 2004, Imaging multiple reflections, the concept: 74th Annual Meeting, SEG, Expanded Abstracts, **23**, 1273–1276.

——, 2006, Imaging of multiple reflections: Geophysics, **71**, no. 4, SI209–SI220, doi:10.1190/1.2215359.

Bernitsas, N., J. Sun, and C. Sicking, 1997, Prism waves–An explanation for curved seismic horizons below the edge of salt bodies: 59th EAGE Conference and Exhibition, EAGE, Extended Abstracts, E038.

Broto, K., and P. Lailly, 2001, Towards the tomographic inversion of prismatic reflections: 71st Annual Meeting, SEG, Expanded Abstracts, 726–729.

Brown, M. P., and A. Guitton, 2005, Least-squares joint imaging of multiples and primaries: Geophysics, **70**, no. 5, S79–S89, doi:10.1190/1.2052471.

Candès, E., L. Demanet, D. Donoho, and L. Ying, 2006, Fast discrete curvelet transforms: Multiscale Modeling and Simulation, **5**, 861–899, doi:10.1137/05064182X.

Cavalca, M., and P. Lailly, 2005, Prismatic reflections for the delineation of salt bodies: 75th Annual Meeting, SEG, Expanded Abstracts, 2550–2553.

——, 2007, Accounting for the definition domain of the forward map in traveltime tomography–Application to the inversion of prismatic reflections: Inverse Problems, **23**, 139–164, doi:10.1088/0266-5611/23/1/007.

Daubechies, I., and G. Teschke, 2005, Variational image restoration by means of wavelets: Simultaneous decomposition, deblurring, and denoising: Applied and Computational Harmonic Analysis, **19**, 1–16, doi:10.1016/j.acha.2004.12.004.

de Hoop, M. V., 1996, Generalization of the Bremmer coupling series: Journal of Mathematical Physics, **37**, 3246–3282, doi:10.1063/1.531566.

Duchkov, A. A., F. Andersson, and M. V. de Hoop, 2010, Discrete, almost symmetric wave packets and multi-scale geometrical representation of (seismic) waves: IEEE Transactions on Geoscience and Remote Sensing, **48**, 3408–3423.

Farmer, P. A., I. F. Jones, H. Zhou, R. I. Bloor, and M. C. Goodwin, 2006, Application of reverse time migration to complex imaging problems: First Break, **24**, 65–73.

Ferguson, R. J., and G. F. Margrave, 2002, Prestack depth migration by symmetric nonstationary phase shift: Geophysics, **67**, 594–603, doi:10.1190/1.1468620.

Gazdag, J., and P. Sguazzero, 1984, Migration of seismic data by phase shift plus interpolation: Geophysics, **49**, 124–131, doi:10.1190/1.1441643.

Hale, D., N. R. Hill, and J. P. Stefani, 1991, Imaging salt with turning seismic waves: 61st Annual Meeting, SEG, Expanded Abstracts, 1171–1174.

Hawkins, K., 1994, The challenge presented by North Sea Central Graben salt domes to all DMO algorithms: First Break, **12**, 327–343.

Hennenfent, G., and F. J. Herrmann, 2006, Seismic denoising with nonuniformly sampled curvelets: Computing in Science and Engineering, **8**, 16–25, doi:10.1109/MCSE.2006.49.

Jiang, Z., 2006, Migration of interbed multiple reflections: 76th Annual Meeting, SEG, Expanded Abstracts, 3501–3505.

Jiang, Z., J. Sheng, J. Yu, G. T. Schuster, and B. E. Hornby, 2007, Migration methods for imaging different-order multiples Geophysical Prospecting, **55**, 1–19, doi:10.1111/j.1365-2478.2006.00598.x.

Jiang, Z., J. Yu, G. T. Schuster, and B. E. Hornby, 2005, Migration of multiples: The Leading Edge, **24**, 315–318, doi:10.1190/1.1895318.

Jin, S., S. Xu, and D. Walraven, 2006, One-return wave equation migration: Imaging of duplex waves: 76th Annual Meeting, SEG, Expanded Abstracts, 2338–2342.

Jones, I. F., M. C. Goodwin, I. D. Berranger, H. Zhou, and P. A. Farmer, 2007, Application of anisotropic 3D reverse time migration to complex North Sea imaging: 77th Annual Meeting, SEG, Expanded Abstracts, 2140–2144.

Kostyukevych, A., N. Marmalevskyi, Y. Roganov, and V. Roganov, 2009, Analysis of azimuthally-dependent transmission coefficients of converted PS-waves for duplex migration on transmitted waves: 79th Annual Meeting, SEG, Expanded Abstracts, 1257–1261.

Link, B., N. Marmalevskyi, Y. Roganov, A. Kostyukevych, and Z. Gornyak, 2007, Direct imaging of subtle, zero-throw vertical faulting—A 3D real-data example: 77th Annual Meeting, SEG, Expanded Abstracts, 2359–2363.

Malcolm, A. E., and M. V. de Hoop, 2005, A method for inverse scattering based on the generalized Bremmer coupling series: Inverse Problems, **21**, 1137–1167, doi:10.1088/0266-5611/21/3/021.

Malcolm, A. E., B. Ursin, and M. V. de Hoop, 2009, Seismic imaging and illumination with internal multiples: Geophysical Journal International, **176**, 847–864, doi:10.1111/j.1365-246X.2008.03992.x.

Marmalevskyi, N., Y. Roganov, Z. Gornyak, A. Kostyukevych, and V. Mershchiy, 2005, Migration of duplex waves: 75th Annual Meeting, SEG, Expanded Abstracts, 2025–2028.

Marmalevskyi, N., Y. Roganov, A. Kostyukevych, and V. Roganov, 2008, Duplex wave migration and interferometry for imaging onshore data without angle limitations: 70th EAGE Conference and Exhibition, EAGE, Extended Abstracts, P273.

Métivier, L., F. Delprat-Jannaud, L. Halpern, and P. Lailly, 2009, 2D nonlinear inversion of walkaway data: 79th Annual Meeting, SEG, Expanded Abstracts, 2342–2346.

Mittet, R., 2002, Multiple suppression by prestack reverse time migration: A nail in the coffin: 64th EAGE Conference and Exhibition, EAGE, Extended Abstracts, P025.

——, 2006, The behaviour of multiples in reverse-time migration schemes: Presented at 68th EAGE Conference and Exhibition, Workshop 6, EAGE.

Downloaded 22 Jun 2011 to 72.93.188.223. Redistribution subject to SEG license or copyright; see Terms of Use at http://segdl.org/

Muijs, R., J. O. A. Robertsson, and K. Holliger, 2007, Prestack depth migration of primary and surface-related multiple reflections: Part I—Imaging: Geophysics, **72**, no. 2, S59–S69, doi:10.1190/1.2422796.
Reiter, E. C., M. N. Toksöz, T. H. Keho, and G. M. Purdy, 1991, Imaging with deep-water multiples: Geophysics, **56**, 1081–1086, doi:10.1190/1.1443119.
Schuster, G. T., J. Yu, J. Sheng, and J. Rickett, 2004, Interferometric/daylight seismic imaging: Geophysical Journal International, **157**, 838–852, doi:10.1111/j.1365-246X.2004.02251.x.
Stolt, R., 2002, Seismic data mapping and reconstruction: Geophysics, **67**, 890–908, doi:10.1190/1.1484532.
Vasconcelos, I., R. Snieder, and B. Hornby, 2007, Target-oriented interferometry—Imaging with internal multiples from subsalt VSP data: 77th Annual Meeting, SEG, Expanded Abstracts, 3069–3073.
Weglein, A., F. B. Araújo, P. M. Carvalho, R. H. Stolt, K. H. Matson, R. T. Coates, D. Corrigan, D. J. Foster, S. A. Shaw, and H. Zhang, 2003, Inverse scattering series and seismic exploration: Inverse Problems, **19**, R27–R83, doi:10.1088/0266-5611/19/6/R01.
Xu, S., and S. Jin, 2006, Wave equation migration of turning waves: 76th Annual Meeting, SEG, Expanded Abstracts, 2328–2331.
——, 2007, An orthogonal one-return wave-equation migration: 77th Annual Meeting, SEG, Expanded Abstracts, 2325–2329.
Youn, O. K., and H. Zhou, 2001, Depth imaging with multiples: Geophysics, **66**, 246–255, doi:10.1190/1.1444901.
Zhang, Y., S. Xu, and G. Zhang, 2006, Imaging complex salt bodies with turning-wave oneway wave equation: 76th Annual Meeting, SEG, Expanded Abstracts, 2323.

Downloaded 22 Jun 2011 to 72.93.188.223. Redistribution subject to SEG license or copyright; see Terms of Use at http://segdl.org/